Chemistry Europe

AWARD

Nominate a Worthy Chemist Chemistry Europe Award

Subject:
chemistry for sustainability, energy, materials, environment

Consists of:
prize money amounting to EUR 10,000, certificate

Deadline:
November 1, 2022

Click here for more info & nomination

Research Article
doi.org/10.1002/cplu.202200262

Chemistry Europe
European Chemical Societies Publishing

www.chempluschem.org

Self-Assembly of Chiro-Optical Materials from Nonchiral Oligothiophene-Porphyrin Derivatives and Random Coil Synthetic Peptides

Katriann Arja,[a] Robert Selegård,[b] Markéta Paloncýová,[c, d] Mathieu Linares,[e] Mikael Lindgren,[f] Patrick Norman,[c] Daniel Aili,[b] and K. Peter R. Nilsson*[a]

Biomimetic chiral optoelectronic materials can be utilized in electronic devices, biosensors and artificial enzymes. Herein, this work reports the chiro-optical properties and architectural arrangement of optoelectronic materials generated from self-assembly of initially nonchiral oligothiophene–porphyrin derivatives and random coil synthetic peptides. The photo-physical- and structural properties of the materials were assessed by absorption-, fluorescence- and circular dichroism spectroscopy, as well as dynamic light scattering, scanning electron microscopy and theoretical calculations. The materials display a three-dimensional ordered helical structure and optical activity that are observed due to an induced chirality of the optoelectronic element upon interaction with the peptide. Both these properties are influenced by the chemical composition of the oligothiophene–porphyrin derivative, as well as the peptide sequence. We foresee that our findings will aid in developing self-assembled optoelectronic materials with dynamic architectonical accuracies, as well as offer the possibility to generate the next generation of materials for a variety of bioelectronic applications.

Introduction

The development of chiral thiophene- or porphyrin-based optoelectronic materials is of great interest due to their numerous potential applications in biosensors, artificial enzymes and electronic devices.[1–6] In this regard, chiral biomolecules have been employed to achieve an induced circular dichroism (ICD) in porphyrins or oligo- and polythiophenes upon interaction with the biomolecular target.[7–18] For instance, porphyrins and polythiophenes have been shown to exhibit ICDs when mixed with DNA or carbohydrates.[7–9,12,16,18] Likewise, a variety of polypeptides have been utilized to achieve an ICD of achiral porphyrins;[7,13–15] whereas synthetic peptides have been employed to induced ICD as well as distinct architectural arrangement in poly- and oligothiophenes.[10,11,17] Thus, through self-assembly of chiral biomolecules and non-chiral optoelectronic elements, chiro-optical materials with distinct optical properties as well as specific structures can be afforded. In addition, covalent attachment of different peptide sequences to π-conjugated molecules have also been applied to generate optoelectronic nanomaterials.[19–21] Chiral porphyrins also play a vital role in several biochemical and biological systems,[22–24] and has therefore been utilized for the development of synthetic biomimetic systems in which the porphyrin moieties act as light-harvesting materials, energy/electron donors and acceptors, or selective coordination and recognition species.[24–30]

Herein, we present the optical- and structural characterization of chiral optoelectronic hybrid materials that are generated by self-assembly of initially random coil synthetic peptides, designed to fold into two different structural motifs and nonchiral oligothiophene–porphyrin molecular scaffolds. The cationic peptide, JR2K (Figure 1A), folds into helix-loop-helix motif and form a four-helix bundle heterodimer with a

[a] Dr. K. Arja, Prof. K. P. R. Nilsson
Division of Chemistry
Department of Physics, Chemistry and Biology
Linköping University
581 83 Linköping (Sweden)
E-mail: peter.r.nilsson@liu.se
[b] Dr. R. Selegård, Prof. D. Aili
Laboratory of Molecular Materials
Division of Biophysics and Bioengineering
Department of Physics, Chemistry and Biology
Linköping University
581 83 Linköping (Sweden)
[c] Dr. M. Paloncýová, Prof. P. Norman
Division of Theoretical Chemistry and Biology
School of Engineering Sciences in Chemistry, Biotechnology and Health
KTH Royal Institute of Technology
106 91 Stockholm (Sweden)
[d] Dr. M. Paloncýová
Regional Centre of Advanced Technologies and Materials
Czech Advanced Technology and Research Institute (CATRIN)
Palacký University Olomouc
779 00 Olomouc (Czech Republic)
[e] Dr. M. Linares
Laboratory of Organic Electronics and Group of Scientific Visualization
Department of Science and Technology (ITN)
Linköping University
601 74 Norrköping (Sweden)
[f] Prof. M. Lindgren
Department of Physics
Norwegian University of Science and Technology
7491 Trondheim (Norway)

Supporting information for this article is available on the WWW under https://doi.org/10.1002/cplu.202200262

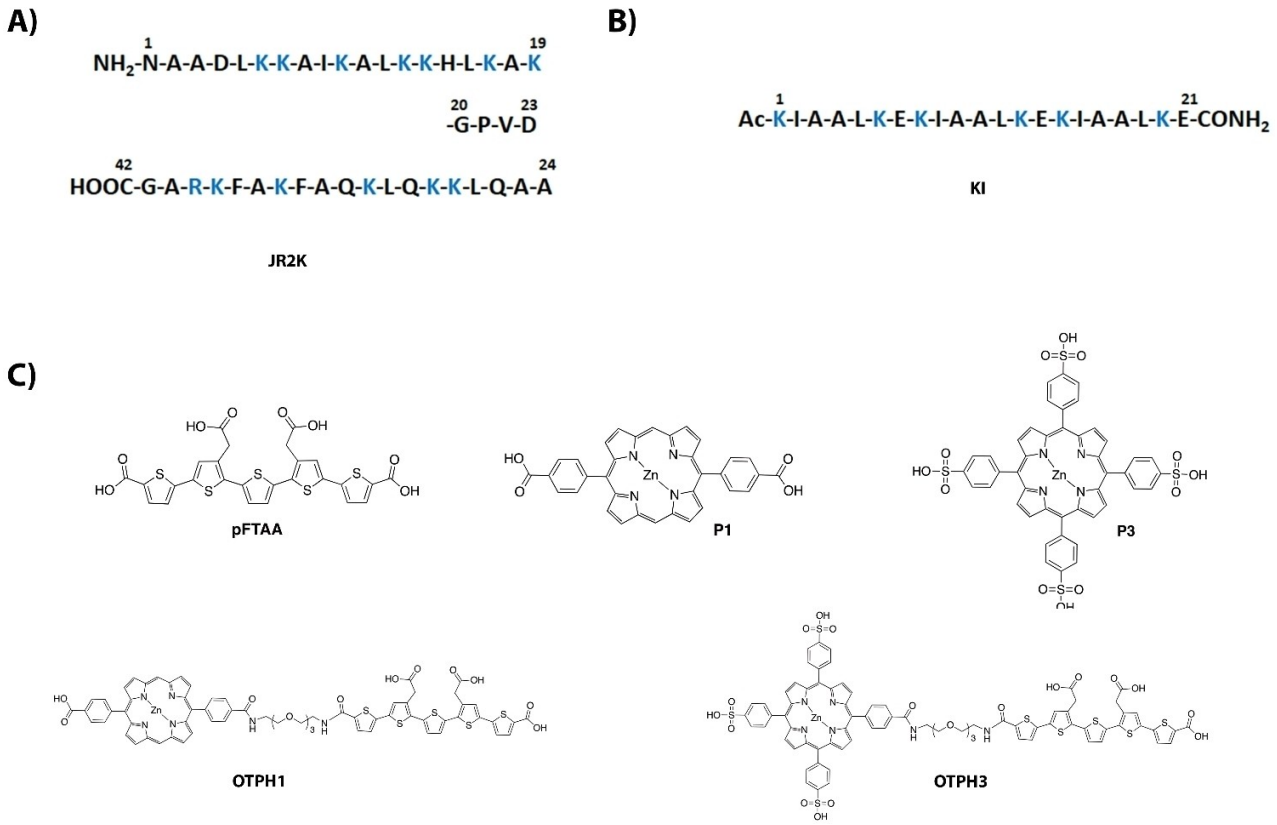

Figure 1. Peptide sequences, chemical structure and photophysical characteristics of the oligothiophenes, porphyrins, and oligothiophene–porphyrin derivates. A) Amino acid sequence of the cationic peptide JR2K. The positively charged residues lysine (K) and arginine (R) are highlighted in blue. **B**) Amino acid sequence of the cationic peptide KI. The positively charged lysine (K) residues are highlighted in blue. **C**) Chemical structures of the oligothiophene, pFTAA, the porphyrin moieties, P1 and P3, and the OTPHs, OTPH1 and OTPH 3.

negatively charged complementary peptide, whereas homodimerization is prevented by electrostatic repulsion at neutral pH.[10,31,32] Analogously, the cationic peptide KI (Figure 1B) will form a coiled coil structure upon addition of a complementary anionic peptide.[33,34] As optoelectronic elements, some recently presented oligothiophene–porphyrin based ligands, OTPH1 and OTPH3 (Figure 1C),[35] were selected, since these anionic materials were expected to form complementary molecular interactions with the cationic peptides. In addition, the pure oligothiophene building block, pFTAA (Figure 1C),[36] as well as the two porphyrin moieties, P1 and P3 (Figure 1C),[35] were included in the study. The photo-physical properties and the architectural arrangement of the self-assembled materials were assessed by a variety of experimental techniques, as well as theoretical calculations. The materials display distinct ordered structures and specific optical activity that were highly influenced by the chemical composition of the oligothiophene–porphyrin derivative, as well as the peptide sequence.

Results and Discussion

Basic photophysical properties

To investigate the interactions between the two different peptides and the optoelectronic molecules, the basic photophysical properties of the molecular components and the assemblies were assessed in terms of the spectral absorption and fluorescence shifts. For the latter also time-resolved properties were explored. Samples were prepared by dissolving the optoelectronic molecules in 20 mM phosphate buffer (pH 7.0) or mixed (1 : 1 molar ratio) with the respective cationic peptide in the same buffer in a concentration range of 2–10 μM. As recently reported,[17] a red-shift of both the absorption- and emission spectra was obtained for p-FTAA when combined with the helix-loop-helix peptide, JR2K, and for the sake of discussion, the spectra are here shown in Figure S1. In contrast, when combined with the coiled coil peptide, KI, the absorption spectrum was unaltered except for an approximately 25% reduction in extinction coefficient (ε) and a concomitant decrease in emission (Supporting Information (SI), Figure S1). The decay times calculated from TC-SPC (time-correlated single photon counting) are shown in Table 1, whereas the raw-data decay traces along with reconvolution fits are displayed in Figure S2A. The fitted traces revealed a decay time of 635 ps for

Table 1. Decay times with and without peptides.

Compound	Decay times [ps] PBS	+ JR2K	+ KI
p-FTAA	635 ± 4	655 ± 5	631 ± 5
P1	2650 ± 29	2590 ± 29	2620 ± 29
OTPH1	1290 ± 14	2350 ± 26	2310 ± 23
P3	1850 ± 88	2150 ± 63	1860 ± 51
OTPH3	1180 ± 9	1960 ± 12	1860 ± 13

pFTAA, with a small increase of 20 ps for the pFTAA–JR2K complex. Within experimental error approximately the same decay time was measured for the pFTAA–KI complex (631 ps). The values of 635 ps for pFTAA alone in buffer was in according to previous data using similar solvents and conditions.[36] Thus, pFTAA seemed to interact rather weakly, but in a different fashion with the two different cationic peptides.

The Zn–porphyrin compounds showed characteristic porphyrin spectra with a strong Soret band around 410–430 nm (P1, P3, OTPH1 and OTPH3 at 409, 420, 415 and 427 nm, respectively). The weaker Q-bands were located around 550–600 nm with the bands of the P3 variants red-shifted (Figure 2). For the optoelectronic molecules, comprising a porphyrin moiety linked to pFTAA, a significant absorption in pFTAA to higher excited states was observed, shown as a broad shoulder in the range 350–500 nm under the Soret band (compare SI, Figure S1). All the emission bands from porphyrin containing moieties were split into two vibrational sub-bands which is well-known for Zn-stabilized porphyrins, meaning that the substitution pattern from P1 (2x – elongated) to P3 (4x – symmetric) did not have a strong influence on the lowest excited state of the ring-structures.[37]

Upon mixing the optoelectronic molecules with the peptide JR2K there were similar red-shifts in bands as observed for pFTAA (SI, Figure S1), especially for the two porphyrin moieties, P1 and P3 (Figure 2A–B). A weak red-shift in absorption was also observed for both the oligothiophene–porphyrin hybrid materials, OTPH1 and OTPH3, with the absorption spectra slightly altered when mixed with JR2K (Figure 2C–D). In addition, upon mixing with JR2K there was an increased emission detected for OTPH1 and OTPH3 (not shown) and concomitantly, a significantly elongated emission decay-time from 1290 to 2350 ps for OTPH1 and from 1180 to 1960 ps for OTPH3 (Table 1, Figure S2). A slight increase in the decay-time was also observed for OTPH3 mixed with the KI peptide whereas for P1 only very minor changes were observed for both peptides. The decay times for all the porphyrin-moieties were in rough agreement with previous results on similar

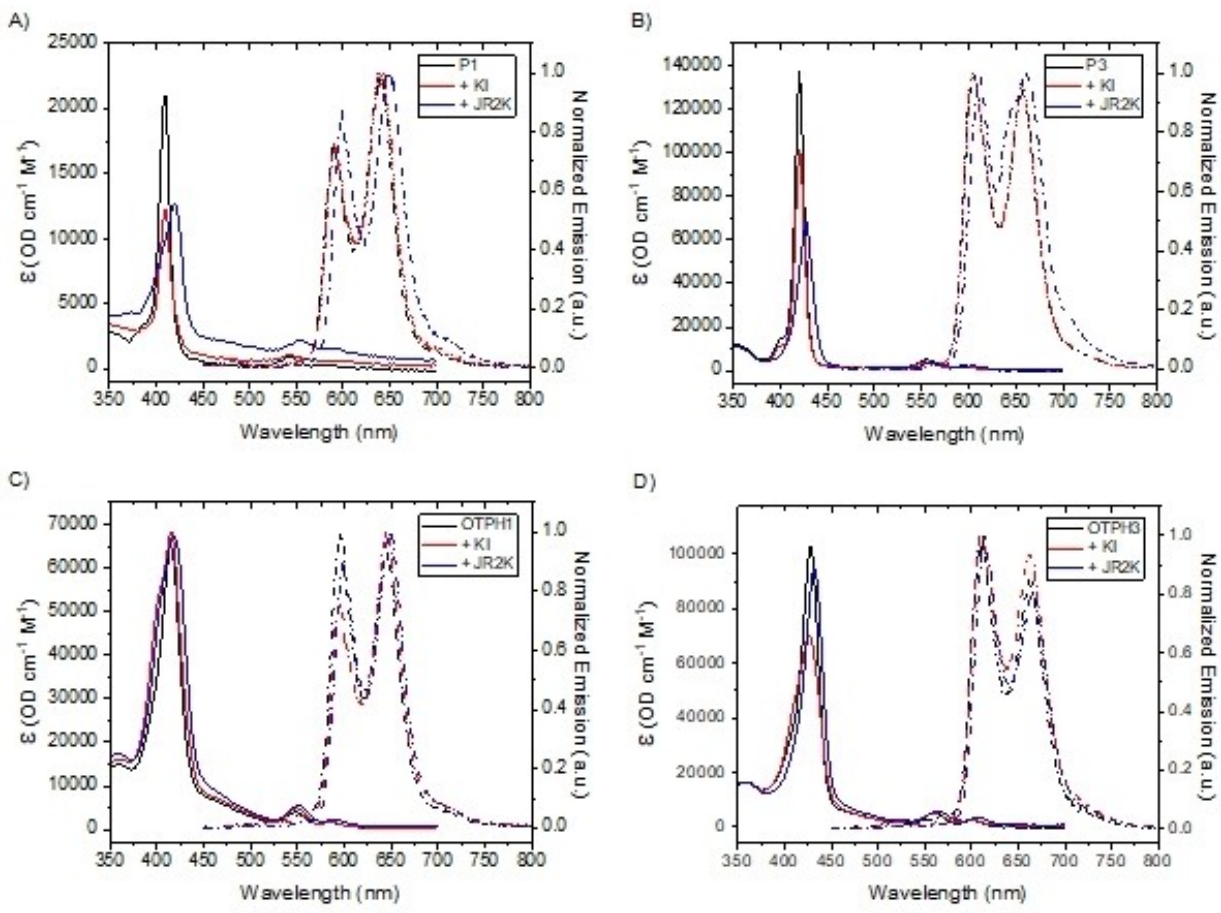

Figure 2. Absorption and emission spectra of the optoelectronic compounds A) P1 **B)** P3 **C)** OTPH1 and **D)** OTPH3. All samples in 20 mM phosphate buffer pH 7.4 or mixed with 10 μM of the respective peptide, JR2K or KI, in the same buffer. The emissions were recorded upon excitation at 435 nm.

compounds with decay times usually in the 1–3 ns range corroborating with the spectral analysis.[38] Overall, the assessment of the optical characteristics for the different optoelectronic molecules when combined with the two peptides, suggested that all the molecules interact with both the peptides but in different fashions.

Characterization of chiral properties

To further investigate the structural properties of the obtained assemblies, circular dichroism (CD) spectra were recorded for all the samples described above. In the absence of peptides, none of the optoelectronic molecules displayed a CD signal in the visible spectral range (SI, Figure S3). In contrast, when combined with JR2K all of the optoelectronic molecules showed an ICD in the visible region (Figure 3A). The interaction between pFTAA and JR2K resulted in a split-type ICD in the π-π^* transition region and the shape and the sign of the ICD pattern (positive/negative Cotton effect) are characteristic of a left-handed helical form of oligo- and polythiophenes.[17,39,40] In contrast, interaction between JR2K with P1 or P3 resulted in a biphasic ICD pattern in the Soret band with negative Cotton effects at shorter wavelengths and positive Cotton effects at longer wavelengths. Similar ICDs have been observed when combining porphyrins with other synthetic peptides, such as poly-L-glutamate, whereas the ICD pattern was reversed when the porphyrin interacts with poly-D-glutamate.[7,14] OTPH1 and OTPH3 displayed a similar ICD pattern (negative/positive Cotton effects) as pFTAA when interacting with JR2K. Overall, the CD experiments verified that all the optoelectronic molecules interacted with JR2K as distinct chiro-optical signals could be attributed to these molecules as a result of the interaction with the peptide.

To reveal the structure of supramolecular assemblies from (induced) CD spectra is a challenging problem in general and which sometimes can be solved by means of theoretical simulations. In this regard, a correlation between the CD-signal from p-FTAA bound to JR2K and the molecular interplay between these two molecular species has been presented in an earlier study.[17] To gain a microscopic understanding of the observed CD signals from the porphyrin moiety bound to JR2K,

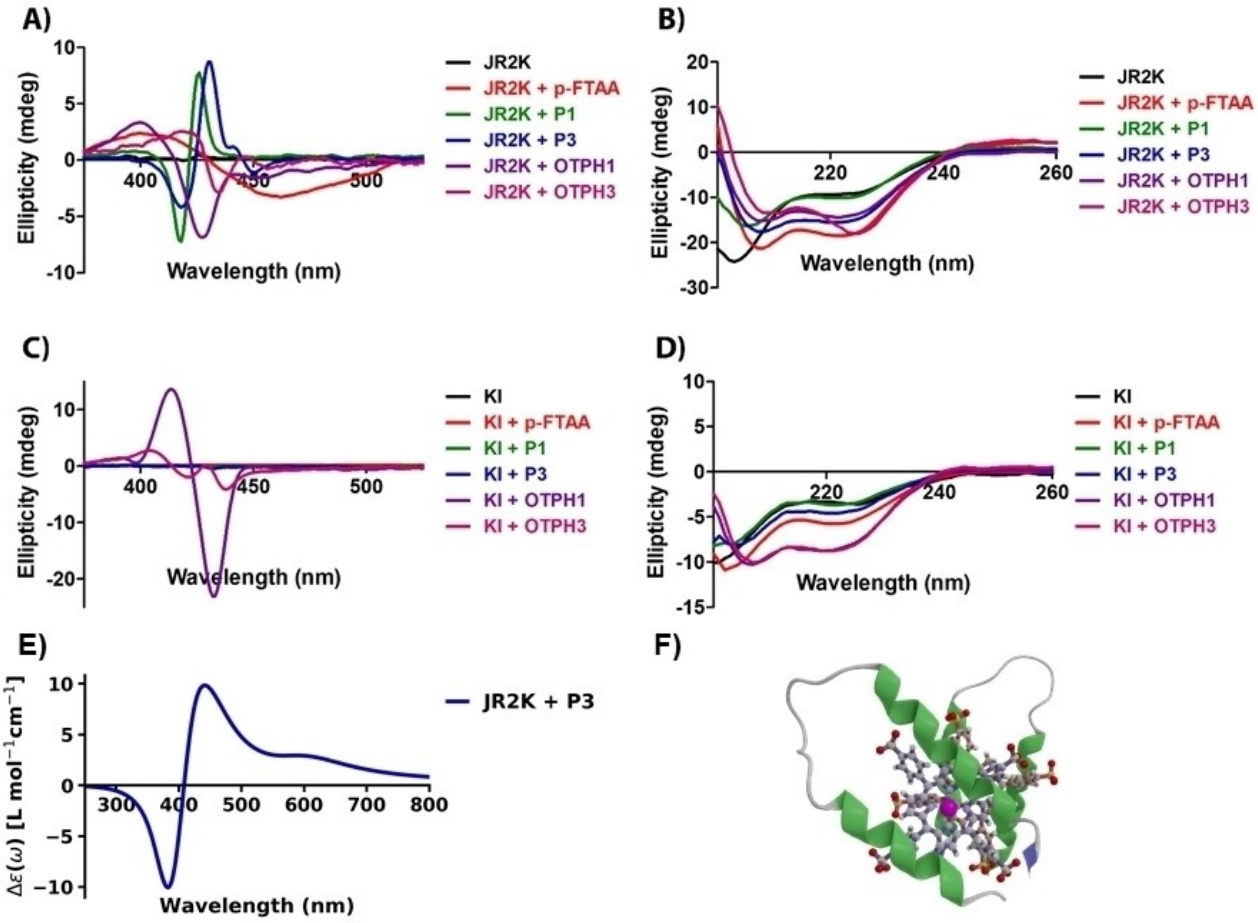

Figure 3. Circular dichroism spectra (CD) of the optoelectronic molecules when combined with the cationic peptides. **A**–**B)** CD spectra of 30 μM of the respective optoelectronic molecule combined with 30 μM JR2K in 20 mM sodium phosphate, pH 7.0. The CD spectra in the visible region (**A**) originate from the optoelectronic molecule, whereas the CD spectra in the UV region (**B**) originate from the peptide (JR2K). **C**–**D)** CD spectra of 30 μM of the respective optoelectronic molecule combined with 30 μM KI in 20 mM sodium phosphate, pH 7.0. The CD spectra in visible spectra region (**C**) originate from the optoelectronic molecules, whereas the CD spectra in the UV region (**D**) originate from the peptide (KI). **E)** CD spectrum of JR2K + P3 calculated as an ensemble average of 35 snapshots. **F)** Representative conformation of a JR2K homodimer interacting with P3.

we chose the P3 ligand as it was seen to be the source of the strongest experimental CD signal, and we investigated the JR2K–P3 heterodimer by a combination of classical and quantum-mechanical molecular modelling. We performed classical force-field molecular dynamics (MD) simulations to study the supramolecular formation followed time-dependent density functional theory (TDDFT) calculations of CD spectra. We refer to the SI for a more complete description of the details of the calculations.

To estimate the dynamics and mutual interactions of JR2K with P3, we started with unbiased all-atom MD simulations. First, the JR2K peptide alone was simulated in water. Its initial double α-helical structure started to disintegrate within the first 10 ns of the simulation, especially in the region of the C-terminal helix (SI, Figure S4), and the α-helical organization was thereafter spontaneously regained and lost during the rest of the simulation.

Second, we added a P3 ligand and let it diffuse towards the JR2K peptide. The negatively charged P3 interacted with the surplus of positively charged lysine (K) residues in JR2K in ways such that the α-helices were stabilized. Three possible resulting conformations were observed namely (i) P3 embedded between the two JR2K helices, (ii) P3 next to the both helices in JR2K, and (iii) P3 interacting only with the N-terminal one of the JR2K helices (Figure 4). We chose structure (ii) for our further studies. In making this choice, we were guided by the bisignate CD signal in the experiment that we thought could stem from the exciton coupling associated with cofacially π-stacked porphyrines. The structure in Figure 4B seemed to offer the best chance to meet this hypothesis.

Third, we investigated an isolated dimer of P3, i.e., in the absence of solvent, counterions, and peptides. We prepared this P3 dimer in a set of configurations with monomers mutually rotated (or twisted) by 10–55°. Using the VeloxChem program,[41] we calculated the CD spectra resulting from this twist-orientation (SI, Figure S5) and identified the structure rotated by 30° as the most relevant one based on the fact that the associated CD spectrum showed to be in good agreement with the experimental one for the JR2K–P3 system.

Fourth, we used this information to prepare a more realistic system composed of a pair of dissolved JR2K–P3 heterodimers with a similar cofacial and twisted organization of the porphyrins and which was simulated using MD under room temperature conditions for over 1 μs. We observed that the JR2K peptide monomers spontaneously rotated with respect to each other to reach a final mutually perpendicular orientation (Figure 5). Associated with this conformational change, the porphyrins also changed their cofacial orientation. For the first ~400 ns they were rotated by the initial ~30° after which a rapid movement was observed and for the last >500 ns, the P3 ligands were mutually rotated by ~130°. Moreover, the P3 ligands were not perfectly stacked with a twisted orientation but rather in a slided configurations with ~5–6 Å between the two Zn atoms. Similarly, to the simulation of a single JR2K with P3, we monitored the interactions of positively charged K residues in JR2K with negatively charged sulphonyl groups in P3.

Fifth, we extracted 35 statistically uncorrelated snapshots from the MD simulation. From these snapshots we extracted the two porphyrins and calculated the CD signals induced by their dynamic structure arrangement (SI, Figure S6). We formed the ensemble average of the spectra as to result in the spectrum presented in Figure 3E. This resulting theoretical CD spectrum is in very good agreement with the experimental observation of a negative Cotton effects at shorter wavelengths and positive Cotton effects at longer wavelengths, which we consider giving a strong corroborating evidence for having revealed the correct supramolecular organization of the JR2K–P3 complex.

The features of the experimental CD spectra for P1 and P3 together with JR2K are nearly identical and it is reasonable to assume that they form very similar complexes. The experimental CD spectra for the OTPH ligands, on the other hand, are substantially less distinct with broader spectral features, suggesting a more stochastic structure arrangement.

Solid evidence for distinct molecular interactions between the anionic optoelectronic molecules and the cationic JR2K could also be observed when analysing the UV-region of the CD spectra (Figure 3B). The spectrum of JR2K in 20 mM phosphate buffer pH 7.0 showed that the peptide lacks defined secondary structure. In contrast, the CD spectra in the far-UV region for JR2K interacting with pFTAA, P3, OTPH1 or OTPH3 displayed strong negative peaks at 208 and 222 nm, indicative of a helical structure (Figure 3B). Thus, the interaction between JR2K and these anionic optoelectronic molecules induced an ordered

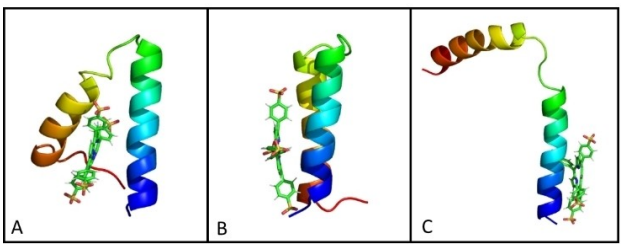

Figure 4. Three types of JR2K–P3 interaction modes: **A)** JR2K with two parallel α-helices and P3 between them, **B)** JR2K with two parallel α-helices and P3 interacting with both of them from one side and **C)** JR2K with two helices in L-shape a P3 interacting with the N-terminal helix. JR2K is shown as cartoon, P3 as sticks. Water is omitted for clarity.

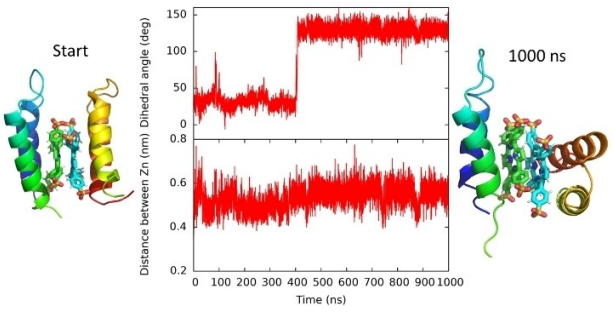

Figure 5. Molecular dynamics simulation of a pair of JR2K–P3 heterodimers. An abrupt structure relaxation is shown after ca. 400 ns after which the supramolecular organization remains stable.

helical structure of the peptide. Interestingly, the ratio of the mean residue ellipticities at 222 nm and 208 nm was very different when JR2K was combined with OTPH3 or OTPH1, respectively. A similar phenomenon has previously been observed for pentameric oligothiophenes with distinct spacing of anionic side chain functionalities along the thiophene backbone,[17] suggesting that the difference in the anionic charges of the porphyrin moiety of OTHP1 and OTPH3 might induce slightly different helical structures of JR2K. In addition, the CD spectrum of JR2K interacting with P3 was also different compared to the spectrum obtained for the peptide interacting with P1 (Figure 3B). Although an alteration in the CD spectrum was observed compared to JR2K alone, the specific signature indicative of helical structure was not observed for JR2K when interacting with P1. The helical structure of the peptide is most likely a result of the stabilizing effect caused by hydrophobic interactions between the nonpolar amino acids and the hydrogen-bonded ion pair complex between the negatively charged substituents of the optoelectronic molecules and the positively charged K groups of the peptide side chains. Since P1 only has two negatively charged substituents, two carboxyl groups, the stabilizing effect will not be as efficient as for the four anionic sulfonic groups of P3. Altogether, the CD measurements for JR2K combined with the optoelectronic molecules suggest that interactions between the negatively charged groups of the optoelectronic molecules and the positively charged amine groups of the lysine side chains in the peptide are responsible for the induced chirality in the optoelectronic molecules, as well as the obtained helical structure of the peptide. Hence, self-assembly of the nonchiral oligothiophene or porphyrin derivatives with JR2K generated chiro-optical hybrid materials with distinct optical properties and specific structures.

When analysing the CD spectra for the optoelectronic elements combined with the second cationic peptide, KI, strikingly different results compared those observed for JR2K were obtained (Figure 3). Firstly, an ICD in the visible region was only seen for OTPH1 or OTPH3 interacting with KI (Figure 3C). Secondly, the strong negative peaks at 208 and 222 nm, indicative of helical structure, were only observed for KI combined with OTPH1 or OTPH3 (Figure 3D). For the pure oligothiophene building block, pFTAA or the two porphyrin moieties, P1 and P3, mixed with KI, the ICD in the visible region as well as the characteristic signature for helical structure were lacking (Figure 3C and 3D). Hence, chiro-optical materials with distinct optical properties and specific structures were only afforded when combining the oligothiophene–porphyrin based ligands with KI.

Dynamic light scattering, rotational anisotropy and scanning electron microscopy

To further investigate the interactions between the optoelectronic molecules and the two peptides, as well as their assembly into more complex structures, dynamic light scattering (DLS) measurements were performed (Figure 6A–C). Individually, the peptides, pFTAA, P1 and OTPH1 produced low scattering intensities ($\leq$20 kHz) and the correlation function showed no presence of large aggregates. Calculated hydrodynamic radius for these individual optoelectronic molecules using a mass weighted algorithm further confirmed their dispersed state (SI, Table S1). In contrast, no scattering signals were obtained for P3 and OTPH3, suggesting that these molecules interacted with the He–Ne laser (632.8 nm) during the DLS measurement. This assumption was also verified with optical experiments showing that, in contrast to P1 and OTPH1, P3 and OTPH3 displayed substantial emission upon excitation at 630 nm (SI, Figure S7). Hence, reliable DLS measurements could not be afforded for P3 and OTPH3, due to fluorescence, allowing the fragment to tumble during its excited state resulting in a loss of coherence with the incident polarized light.

Combining KI with pFTAA or OTPH1 resulted in similar scattering intensities and correlation functions as the molecules alone, indicating that no large assemblies were formed when these optoelectronic molecules were interacting with KI (Figure 6). Slightly larger assemblies were observed for the combination of P1 and KI. The interaction between P3 or OTPH3 and KI could not be assessed due to the lack of scattering signal (Figure 6C) due to their absorption of the laser light. When combined with KI considerable emission upon excitation at 630 nm were seen for both P3 and OTPH3 (SI, Figure S7). The interaction of JR2K and pFTAA did not result in any large assemblies, whereas P1 and JR2K formed slightly larger complexes. No reliable scattering signal could be achieved for P3 mixed with JR2K. However, the combinations of JR2K with OTPH1 and OTPH3 produced very high scattering intensities as well as a dramatic decrease in solution dynamics, indicating the formation of micrometer large assemblies (Figure 6 and SI, Table S1). Remarkably, the previously observed non-coherence for OTPH3 did not appear to influence the measurement, which might be due to altered photophysical characteristics of the ligand that are related to a distinct molecular arrangement of OTPH3 when interacting with JR2K. OTPH3 mixed with JR2K also displayed less emission than OTPH3 in buffer or the ligand mixed with KI, when excited at 630 nm (SI, Figure S7).

Using fluorescence polarization mode of detection (Figure 6) no major differences were seen for pFTAA alone or when combined with KI, further confirming that the interaction between these two molecules is relatively weak. In contrast, pFTAA combined with JR2K showed a clear difference in rotational anisotropy (Figure 6D), indicative of a slower tumbling (Figure 6D). Fitting the anisotropy decay of pFTAA with or without KI gave a rotational diffusion time of 640 ($\pm$60) ps. However, for pFTAA interacting with JR2K the decay time was too short to resolve the local tumbling of as the anisotropy decay never reached to zero, which is typically seen in time-resolved fluorescence anisotropy experiments of large protein aggregates.[42] Similar results were also obtained using the other optoeletronic molecules when combined with both the peptides (Figure S8). Taken together the time-resolved results concludes that some of the optoelectronic molecules interacted with the peptides in distinct fashions and that these inter-

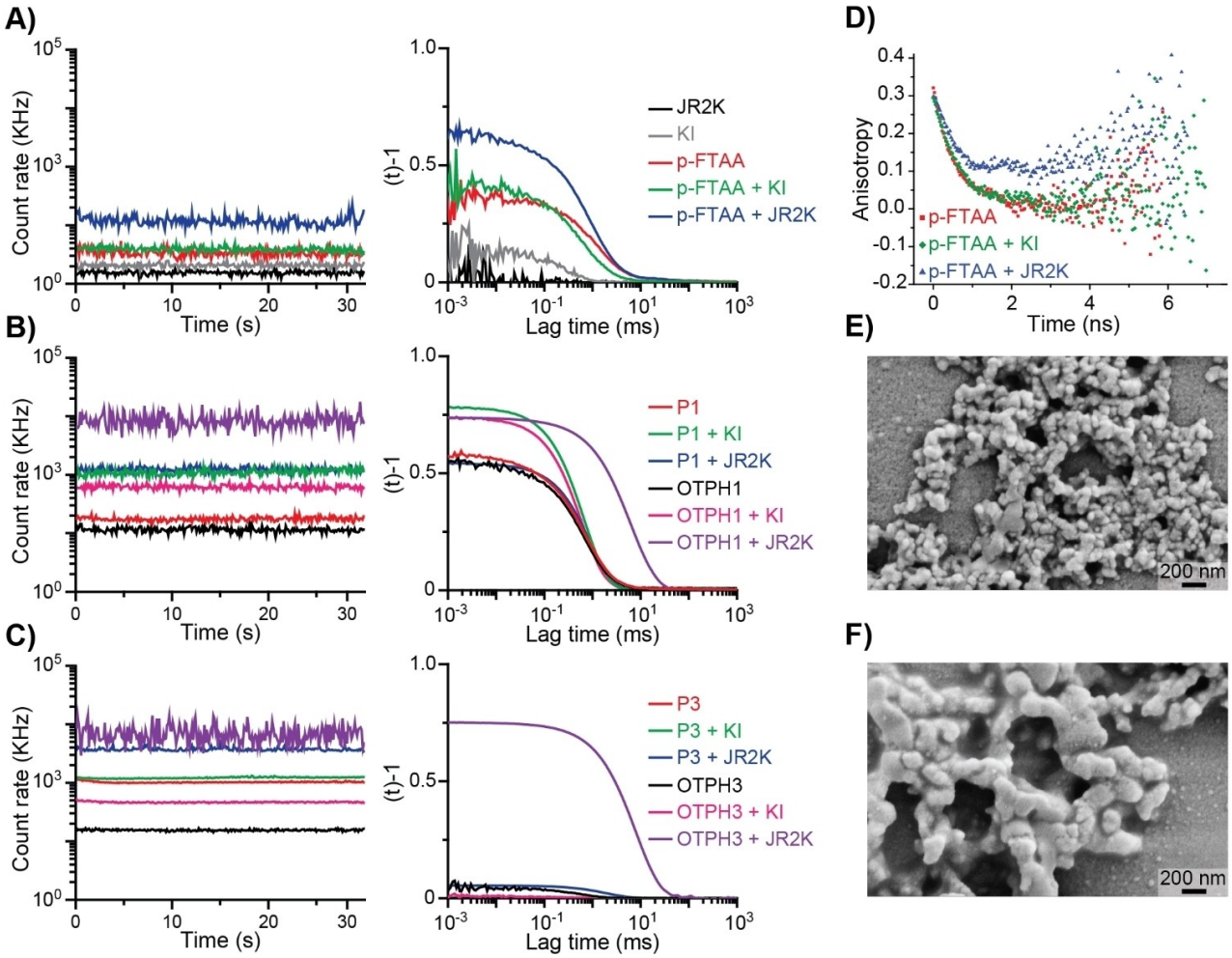

Figure 6. DLS, rotational anisotropy and scanning electron microscope measurements of the optoelectronic molecules mixed with the cationic peptides. **A–C)** Scattering intensities (left panel) and resulting correlation functions (right panel) recorded by dynamic light scattering measurements of 30 μM peptide and 30 μM optoelectronic molecule. **A**) JR2K, KI and p-FTAA alone and in combinations. **B**) P1 and OTPH1 alone and in combinations with peptides. **C**) P3 and OTPH3 alone and in combinations with peptides. **D**) Time-resolved anisotropy measurements of p-FTAA with and without JR2K and KI (λ_{ex} = 403 nm; λ_{em} = 530 nm). **E–F**) Scanning electron microscope (SEM) micrographs of JR2K combined with OTPH1 **(E)** and JR2K combined with OTPH3 **(F)**.

actions fine-tuned the photophysical properties of the optoelectronic molecules

According to the DLS measurement, OTPHs seemed to form different molecular assemblies when interacting with JR2K and KI. Therefore, assemblies that were achieved by adding samples dissolved in phosphate buffer onto conductive carbon tabs and air-dried overnight in room temperature were imaged using scanning electron microscopy (SEM) (Figure 6E and 6F). According to the DLS measurement, the KI peptide did not form any large assemblies when combined with OTPH1 and OTPH3 and no structures could be observed by SEM (data not shown). In contrast, assemblies constituted of JR2K combined with OTPH1 produced spherical-like particles with an approximate size of 100 nm in a dry state, whereas JR2K combined with OTPH3 resulted in slightly larger amorphous structures with an approximate size of $\geq$200 nm. Thus, in accordance with the DLS measurements, larger distinct architectonical assemblies were obtained for the OTPHs mixed with JR2K.

Conclusion

In conclusion, we have shown that materials with specific chiro-optical properties and distinct structures can be generated from non-covalent self-assembly of nonchiral oligothiophene/porphyrin based optoelectronic elements and synthetic peptides with an initial random coil structural arrangement. In addition, both the chiro-optical properties and the structure of the molecular assemblies are influenced by the chemical composition of the oligothiophene–porphyrin derivative, as well as the peptide sequence. These findings might aid in the development of novel self-assembled optoelectronic materials with dynamic architectonical precision, as well as offer the possibility to realize novel materials for a variety of bioelectronic applications.

Experimental Section

Additional figures are given in the Supporting Information (SI) and full experimental details are outlined below.

Synthesis of optoelectronic molecules and peptides

p-FTAA, P1, P3, OTPH1 and OTPH3 were synthesized as reported previously.[35,36,43] The peptide JR2K (H2N–NAADLKKAIKALKKHLKAKGPVDAAQLKKQLKQAFKAFKRAG–CO-OH) was synthesized as described earlier.[10,17] The peptide KI (Ac–KIAALKEKIAALKEKIAALKE–CONH2) was synthesized using standard Fmoc-chemistry on a H-Rink-amide (ChemMatrix) resin in a 100 μM scale. All amino acid couplings were performed with a fourfold excess of amino acids (Iris biotech GmBH), O-(1H-6-Chlorobenzotriazole-1-yl)-1,1,3,3-tetramethyluronium hexafluoro-phosphate (HCTU, Iris biotech GmBH) and an eightfold excess of N, N-diisopropylethylamine (DIPEA). N-terminal was acetylated using acetic anhydride in DMF (1:1, v/v) and cleaved from the solid support using a mixture of trifluoracetic acid (TFA), triisopropylsi-lane and ddH2O (95:2.5:2.5, v/v/v) for 2 hours followed by filtration and evaporation of the solvent. The crude peptide was precipitated twice in cold diethyl ether and purified using an aqueous gradient of acetonitrile with 0.1% TFA on a reversed phase column coupled to semi-preparative HPLC system (Ultimate 3000, Dionex, Thermo fisher scientific, Waltham, USA). Mass identification was confirmed by MALDI-TOF MS using α-cyano-4-hydroxycinnamic acid as matrix (SI, Figure S9).

Optical characterization of the optoelectronic molecules towards JR2K and KI

JR2K and KI was dissolved in buffer (20 mM phosphate, pH 7.0) to a final concentration of 60 μM. The optoelectronic molecules were dissolved in de-ionized water to a concentration of 1.5 mM. The respective optoelectronic molecule was mixed with JR2K solution, KI solution or buffer (20 mM phosphate, pH 7.0) to generate the desired concentration (30 μM of LCO and 0 or 30 μM peptide) and incubated for 10 min. The absorption-, excitation- and emission spectrum for each probe were collected using a Tecan Infinite M1000 Pro microplate reader (Tecan, Männedorf, Switzerland) and CD spectra were recorded with a Chirascan (Applied Photophysics, Leatherhead, U.K.) using a 5 mm or a 1 cm quartz cell.

Lifetimes, anisotropy and quantum yield measurements

Time correlated single photon counting (TC-SPC) and time-resolved anisotropy measurements were carried out using an IBH photon counting spectrometer equipped with polarizers. Samples were prepared from 1.5 mM stock solutions with the concentrations decreased to 5 μM (each of the fluorescent ligand and the peptides) using 3 ml suprasil quartz cuvettes. The quantum yields were measured using a Shimadzu UV-1601PC absorbance spectrometer in conjunction with a PTI quantamaster 8075-22 (Horiba) for steady state fluorescence. Further details on the set-ups and data analysis have been reported elsewhere.[42,44]

Dynamic light scattering (DLS)

DLS measurements were performed with an ALV/DLS/SLS-5022F system from ALV-GmbH (Germany). The He–Ne laser was operated at 632.8 nm and the scattered light was detected perpendicular to the incident laser beam. Samples was prepared as described above. Buffer (phosphate, 20 mM, pH 7.4) and peptides were filtrated through a 0.22 μm low protein binding filter and samples were tempered to 21.5 °C prior to measurements. All measurements were repeated 10 times and the collected data averaged and was fitted to a linear mass-weighted algorithm.

Scanning electron microscopy (SEM)

SEM micrographs were acquired with a LEO 1550 Gemini from Zeiss (Germany) operating at 5 kV. Samples of 30 μM JR2K and 30 μM OTPH1/3 dissolved in phosphate buffer (10 mM, pH 7.4) were added onto conductive carbon tabs and air-dried overnight in room temperature. Prior to measurements a thin layer of platinum was sputtered onto the samples.

Computational setup

Parameterization: The topology for JR2K was built in the Amber14SB[45] force field (FF) with use of the Gromacs tool pdb2gmx and from a structure downloaded from PDB database as 4ZF6 with expected protonation of pH 7.4 (HIS charge 0, total charge of JR2K +11). The toopology for P3 was built in the General Amber FF (GAFF)[46] with the expected charge −4 in pH 7.4. The Metal Center Parameter Builder (MCPB)[47] was used for obtaining the topology. In MCPB, the geometry was optimized at the B3LYP/cc-pVDZ level of theory. Bond- and angle-associated force constants were obtained from frequency calculations at the B3LYP/6-31G* level of theory and partial charges were obtained by the RESP procedure[48] with an electrostatic potential calculated at the level of HF/6-31G*, as recommended in the RESP protocol. Further, we focused on parameterization of rotation of phenyl groups and the twisting of the porphyrin plane (SI, Figure S10). For rotation of phenyl rings, we performed relaxed potential energy scan (PES) at the B3LYP/cc-pVDZ level of theory in Gaussian[49] as well as PES in molecular mechanics (MM) with the topology obtained from MCPB. Due to high energy barriers for full rotation (around 0° and 180°), we focused mostly on the representation of conformations around 90°, so the fitting was performed in angle regions of 15° to 160° and 220° to 325°. For the calculation of the barrier for the twisting of the porphyrin plane, we used relaxed structures from MM PES and calculated single point energies on those. MM optimization of the structure of P3 in vacuum using the obtained parameters resulted in a structure very similar to the one optimized at the QM level (SI, Figure S10).

MD simulations

All MD simulations were performed using GROMACS 2018.1.[50] Initially, models of JR2K and P3 in a desired conformation were built and afterwards the systems were solvated using the TIP3P water model[51] and neutralized by addition of Cl^- ions. The MD simulations were performed with periodic boundary conditions applied in all directions, with the Nosé-Hoover thermostat[52,53] set to 310 K and the isotropic Parrinello-Rahman[54] barostat set to 1.0 bar. Non-covalent interactions were treated explicitly up to 1.1 nm and beyond which a particle-mesh-Ewald summation[55] was applied for Coulombic interactions and van der Waals interactions were cut-off. All bonds were constrained by the LINCS algorithm.[56] All simulations were performed with a 2 fs time step. First, a single JR2K chain was subjected to an unbiased 100 ns simulation in order to evaluate its secondary structure stability. Afterwards, JR2K and P3 were simulated together with initial random mutual position (in seven replicas), and we performed the first 10 ns of the MD simulations with constraints applied on the JR2K backbone in order to preserve its secondary structure, followed by 20 ns of free simulations without any constraints. From these simulations, we

extracted a snapshot of P3 interacting with both JR2K helices via electrostatic interactions with K and R residues (SI, Figure S11).

We proceeded further with two different approaches. First, we placed another P3 molecule to the JR2K–P3 assembly in order to stack with the first P3 molecule. Afterwards, we added second JR2K (with mutual orientation to P3 taken from initial JR2K–P3 assembly) to obtain a JR2K–P3 heterodimer. After an MD simulation, we extracted several snapshots for CD spectra calculations, but we were not able to access experimentally relevant structures by this approach, therefore we moved to a different strategy, focusing first on finding a proper conformation of a P3 dimer. This strategy was more successful, creating a dimer by duplicating, shifting and rotating a P3 molecule. The second P3 molecule was rotated by 10–55° and the CD spectra of these dimers were calculated. Taking into account the experimental CD spectra, for further simulations we used the dimer structure rotated by 30°. The final structure for the MD simulation was prepared in Pymol.[57] The P3 dimer rotated by 30° was used as a start and the JR2K structures were added by aligning the structure of each P3 molecule from the dimer with the P3 molecule from the final snapshot of the simulation of single P3 interacting with single JR2K. First, we performed 250 ns of MD simulations with constraints applied on P3 nitrogens in order to equilibrate the JR2K–P3 interactions and then we performed 1 μs of unbiased MD simulations (SI, Figure S11). We prepared and simulated all four possible mutual JR2K orientations (based on C4 symmetry of P3), but due to the rotations of JR2Ks during the following simulations, we further worked with the JR2Ks starting parallel to each other.

CD spectra calculations

All CD spectra were calculated using the VeloxChem software.[58] Extracted P3 dimer snapshots were modified by replacing the sulphonyl groups by methyls. The rotatory strengths of 20 excited states were calculated at the B3LYP/def2-SVP level of theory. The spectra were constructed with use of a Lorentzian line broadening of 0.3 eV. The final resulting CD spectrum was calculated as an average of all calculated snapshot spectra.

Acknowledgements

Our work was supported by the Swedish Research Council (Grant Nos. 621-2013-4754, 2016-00748, and 2018-4343), the Swedish e-Science Research Centre (SeRC), and the Swedish Foundation for Strategic Research (FFL15-0026). MP acknowledges the support from the Ministry of Education, Youth and Sports of the Czech Republic (ERDF/ESF "Nano4Future" Grant CZ.02.1.01/0.0/0.0/16_019/0000754) and project HPC-EUROPA3 INFRAIA-2016-1-730897 with support of the EC Research Innovation Action under the H2020 Programme. We also acknowledge the provision of super-computer resources from the Swedish National Infrastructure for Computing (SNIC).

Conflict of Interest

The authors declare no conflict of interest.

Data Availability Statement

The data that support the findings of this study are available from the corresponding author upon reasonable request.

Keywords: circular dichroism · oligothiophene · porphyrin · self-assembly · synthetic peptides

[1] M. Lemaire, D. Delabouglise, R. Garreau, A. Guy, J. J. Roncali, *Chem. Soc., Chem. Commun.* **1988**, *10*, 658–661.
[2] M. Andersson, P. O. Ekeblad, T, Hjertberg, O. Wennerström, O. Inganäs, *Polym. Commun.* **1991**, *32*, 546–548.
[3] M. M. Bouman, E. W. Meijer, *Adv. Mater.* **1995**, *7*, 385–387.
[4] G. Bidan, S. Guillerez, V. Sorokin, *Adv. Mater.* **1996**, *8*, 157–160.
[5] F. Andreani, L. Angiolini, D. Caretta, E. Salatelli, *J. Mater. Chem.* **1998**, *8*, 1109–1111.
[6] X. Huang, K. Nakanischi, N. Berova, *Chirality* **2000**, *12*, 237–255.
[7] R. F. Pasternack, A. Giannetto, *J. Am. Chem. Soc.* **1991**, *113*, 7799–780.
[8] P. C. Ewbank, G. Nuding, H. Suenaga, R. D. McCullough, S. Shinkai, *Tetrahedron Lett.* **2001**, *42*, 155–157.
[9] H. A. Ho, M. Boissinot, M. G. Bergeron, G. Corbeil, K. Dore, D. Boudreau, M. Leclerc, *Angew. Chem. Int. Ed.* **2002**, *41*, 1548–1551; *Angew. Chem.* **2002**, *114*, 1618–1621.
[10] K. P. R. Nilsson, J. Rydberg, L. Baltzer, O. Inganäs, *Proc. Natl. Acad. Sci. USA* **2003**, *100*, 10170–10174.
[11] K. P. R. Nilsson, J. Rydberg, L. Baltzer, O. Inganäs, *Proc. Natl. Acad. Sci. USA* **2004**, *101*, 11197–11202.
[12] T. Sanji, N. Kato, M. Tanaka, *Org. Lett.* **2005**, *8*, 235–238.
[13] J. R. Dunetz, C. Sandstrom, E. R. Young, P. Baker, S. A. Van Name, T. Cathopolous, R. Fairman, J. C. de Paula, K. S. Åkerfeldt, *Org. Lett.* **2005**, *7*, 2559–2561.
[14] B. C. Kovaric, B. Kokona, A. D. Schwab, M. A. Twomey, J. C. de Paula, R. Fairman, *J. Am. Chem. Soc.* **2006**, *128*, 4166–4167.
[15] A. Li, L. Zhao, J. Hao, R. Ma, Y. An, L. Shi, *Langmuir* **2014**, *30*, 4797–4805.
[16] Y. Cao, Y. Duan, L. Han, S. Che, *Chem. Commun.* **2017**, *53*, 5641–5644.
[17] R. Selegård, Z. Rouhbakhsh, H. Shirani, L. B. G. Johansson, P. Norman, M. Linares, D. Aili, K. P. R. Nilsson, *Macromolecules* **2017**, *50*, 7102–7110.
[18] N. Kaerkitcha, T. Sagawa, *Photochem. Photobiol. Sci.* **2018**, *17*, 342–351.
[19] R. J. Kumar, J. M. MacDonald, T. B. Singh, L. J. Waddington, A. B. Holmes, *J. Am. Chem. Soc.* **2011**, *133*, 8564–8573.
[20] R. Matmour, I. De Cat, S. J. George, W. Adriaens, P. Leclère, P. H. H. Bomans, N. A. J. M. Sommerdijk, J. C. Gielen, P. C. M. Christianen, J. T. Heldens, J. C. M. van Hest, D. W. P. M. Löwik, S. De Feyter, E. W. Meijer, A. P. H. J. Schenning, *J. Am. Chem. Soc.* **2008**, *130*, 14576–14583.
[21] S. R. Diegelmann, J. M. Gorham, J. D. Tovar, *J. Am. Chem. Soc.* **2008**, *130*, 13840–13841.
[22] J. Deisenhofer, O. Epp, K. Miki, R. Huber, H. Michel, *Nature* **1985**, *318*, 618–624.
[23] J. Barber, B. Andersson, *Nature* **1994**, *370*, 31–34.
[24] J. Xiong, W. M. Fischer, K. Inoue, M. Nakahara, C. E. Bauer, *Science* **2000**, *289*, 1724–1730.
[25] M. K. Panda, K. Ladomenou, A. G. Coutsolelos, *Chem. Rev.* **2012**, *256*, 2601–2627.
[26] X.-S. Ke, B.-Y. Yang, X. Cheng, S. L.-F. Chan, J.-L. Zhang, *Chem. Eur. J.* **2014**, *20*, 4324–4333.
[27] N. L. Bill, M. Ishida, Y. Kawashima, K. Ohkubo, Y. M. Sung, V. M. Lynch, J. M. Lim, D. Kim, J. L. Sessler, S. Fukuzumi, *Chem. Sci.* **2014**, *5*, 3888–3896.
[28] T. Tanaka, A. Osuka, *Chem. Soc. Rev.* **2015**, *44*, 943–969.
[29] J. Tang, J.-J. Chen, J. Jing, J.-Z. Chen, H. Lv, Y. Yu, P. Xu, J.-L. Zhang, *Chem. Sci.* **2014**, *5*, 558–566.
[30] H. Lu, N. Kobayashi, *Chem. Rev.* **2016**, *116*, 6184–6261.
[31] S. Olofsson, G. Johansson, L. Baltzer, *J. Chem. Soc.-Perkin Trans.* **1995**, *2*, 2047–2056.
[32] L. Baltzer, H. Nilsson, J. Nilsson, *Chem. Rev. (Washington, D.C.)* **2001**, *101*, 3153–3163.
[33] C. Aronsson, S. Danmark, F. Zhou, F. P. Öberg, K. Enander, H. Su, D. Aili, *Sci. Rep.* **2015**, *5*,14063.
[34] S. Danmark, C. Aronsson, D. Aili, *Biomacromolecules* **2016**, *17*, 2260–2267.
[35] K. Arja, M. Elgland, K. P. R. Nilsson, *Front. Chem.* **2018**, *6*, 391.

[36] A. Åslund, C. J. Sigurdson, T. Klingstedt, S. Grathwohl, T. Bolmont, D. L. Dickstein, E. Glimsdal, S. Prokop, M. Lindgren, P. Konradsson, D. M. Holtzman, P. R. Hof, F. L. Heppner, S. Gandy, M. Jucker, A. Aguzzi, P. Hammarström, K. P. R. Nilsson, *ACS Chem. Biol.* **2009**, *4*, 673–684.
[37] P. Sen, C. Hirel, C. Andraud, C. Aronica, Y. Bretonnière, A. Mohammed, H. Ågren, B. Minaev, V. Minaeva, G. Baryshnikov, H.-S. Lee, J. Duboisset, M. Lindgren, *Materials (Basel)* **2010**, *3*, 4446–4475.
[38] B. Minaev, M. Lindgren, *Sensors* **2009**, *9*, 1937–1966.
[39] B. M. W. Langeveld-Voss, R. A. J. Janssen, M. P. T. Christiaans, S. C. J. Meskers, H. P. J. M. Dekkers, E. W. Meijer, *J. Am. Chem. Soc.* **1996**, *118*, 4908–4909.
[40] B. M. W. Langeveld-Voss, M. P. T. Christiaans, R. A. J. Janssen, E. W. Meijer, *Macromolecules* **1998**, *31*, 6702–6704.
[41] Z. Rinkevicius, X. Li, O. Vahtras, K. Ahmadzadeh, M. Brand, M. Ringholm, N. H. List, M. Scheurer, M. Scott, A. Dreuw, P. Norman, *WIREs Comput. Mol. Sci.* **2020**, *10*, e1457.
[42] M. Lindgren, P. Hammarström, *FEBS J.* **2010**, *277*, 1380–1388.
[43] K. Arja, D. Sjölander, A. Åslund, S. Prokop, F. L. Heppner, P. Konradsson, M. Lindgren, P. Hammarström, K. O. A. Åslund, K. P. R. Nilsson, *Macromol. Rapid Commun.* **2013**, *34*, 723–730.
[44] C. Gustafsson, H. Shirani, P. Leira, D. R. Rehn, M. Linares, P. Norman, M. Lindgren, *ChemPhysChem* **2021**, *22*, 323–335.
[45] J. A. Maier, C. Martinez, K Kasavajhala, L. Wickstrom, K. E. Hauser, C. Simmerling, ff14SB: Improving the Accuracy of Protein Side Chain and Backbone Parameters from ff99SB. *J. Chem. Theory Comput.* **2015**, *11*, 3696–3713.
[46] J. Wang, R. M. Wolf, J. W. Caldwell, P. A. Kollman, D. A. Case, *J. Comput. Chem.* **2004**, *25*, 1157–1174.
[47] P. Li, K. M. Merz, *J. Chem. Inf. Model.* **2016**, *56*, 599–604.
[48] J. Wang, P. Cieplak, P. A. Kollman, *J. Comput. Chem.* **2000**, *21*, 1049–1074.
[49] M. J. Frisch, G. W. Trucks, H. B. Schlegel, G. E. Scuseria, M. A. Robb, J. R. Cheeseman, G. Scalmani, et al. *Gaussian 16*, **2016**, Revision B.01.
[50] D. Van der Spoel, E. Lindahl, B. Hess, G. Groenhof, A. E. Mark, H. J. C. Berendsen, *J. Comput. Chem.* **2005**, *26*, 1701–1718.
[51] S. R. Durell, B. R. Brooks, A. Ben-Naim, *J. Phys. Chem.* **1994**, *98*, 2198–2202.
[52] S. Nosé, *J. Chem. Phys.* **1984**, *81*, 511–519.
[53] W. G. Hoover, *Phys. Rev. A* **1985**, *31*, 1695–1697.
[54] M. Parrinello, A. Rahman, *J. Appl. Phys.* **1981**, *52*, 7182–7190.
[55] T. Darden, D. York, L. Pedersen, *J. Chem. Phys.* **1993**, *98*, 10089–10092.
[56] B. Hess, H. Bekker, H. J. C. Berendsen, J. G. E. M. Fraaije, *J. Comput. Chem.* **1997**, *18*, 1463–1472.
[57] The PyMOL Molecular Graphics System, Version 1.8. **2015**, Schrodinger, LLC.
[58] Z. Rinkevicius, X. Li, O. Vahtras, K. Ahmadzadeh, M. Brand, M. Ringholm, N. Holmgaard List, M. Scheurer, M. Scott, A, Dreuw, P. Norman, *Wiley Interdiscip. Rev.: Comput. Mol. Sci.* **2020**, *10*, e1457.

Manuscript received: August 8, 2022
Revised manuscript received: September 1, 2022
Accepted manuscript online: September 2, 2022

RESEARCH ARTICLE

Chiral construction: By mixing anionic oligothiophene–porphyrin derivatives and cationic synthetic peptides, self-assembled optoelectronic materials with distinct photophysical properties and specific architectonical arrangement can be afforded. The chemical composition of the oligothiophene–porphyrin derivative, as well as the sequence of the peptide, had large effects on the induced circular dichroism and the structure of the self-assembled supramolecular structures.

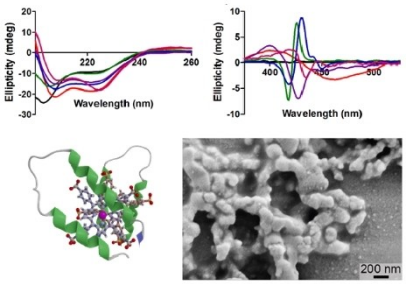

*Dr. K. Arja, Dr. R. Selegård, Dr. M. Paloncýová, Dr. M. Linares, Prof. M. Lindgren, Prof. P. Norman, Prof. D. Aili, Prof. K. P. R. Nilsson**